PRINCIPAL STRESS PORE PRESSURE PREDICTION:

UTILIZING DRILLING MEASUREMENTS TO PREDICT PORE PRESSURE

A Thesis

by

KYLE WADE RICHARDSON

Submitted to the Office of Graduate Studies of
Texas A&M University
in partial fulfillment of the requirements for the degree of

MASTER OF SCIENCE

May 2008

Major Subject: Mechanical Engineering

PRINCIPAL STRESS PORE PRESSURE PREDICTION:

UTILIZING DRILLING MEASUREMENTS TO PREDICT PORE PRESSURE

A Thesis

by

KYLE WADE RICHARDSON

Submitted to the Office of Graduate Studies of
Texas A&M University
in partial fulfillment of the requirements for the degree of

MASTERS OF SCIENCE

Approved by:

Co-Chairs of Committee,	Egidio Marotta
	Thomas Lalk
Committee Member,	Andreas Kronenberg
Head of Department,	Dennis O'Neal

May 2008

Major Subject: Mechanical Engineering

ABSTRACT

Principal Stress Pore Pressure Prediction: Utilizing Drilling Measurements to Predict Pore Pressure. (May 2008)

Kyle Wade Richardson, B.S., Texas A&M University

Co-Chairs of Advisory Committee: Dr. Egidio Marotta
Dr. Thomas Lalk

A novel method of predicting pore pressure has been invented. The method utilizes currently recorded drilling measurements to predict the pore pressure of the formation through which the bit is drilling. The method applies Mohr's Theory to describe the stresses at the bottom of the borehole. From the stress state and knowledge of Mohr's Envelope, the pore pressure is predicted. To verify the method, a test procedure was developed. The test procedure enabled systematic collection and processing of the drilling data to calculate the pore pressure prediction. The test procedure was then applied to industry data that was recorded at the surface. The industry data were composed of wells from different geographical regions.

Two conclusions were deduced from the research. First, Mohr's Theory indicates that the model is valid. Second, because of too much variation in the torque measurements the model cannot be proved and requires further investigation.

ACKNOWLEDGEMENTS

To my committee, Dr. M, Dr. Lalk, and Buddy, thank you for the great laughs and thoughtful insight. Thanks to Carlos, Dong, Scott, and John for working with me on this project.

To my friends and colleagues who encouraged me to pursue my Master of Science in Mechanical Engineering; because of you a world of knowledge and opportunity was revealed to me.

Finally to my family, thanks for the encouragement and help through college. Your support was always known and appreciated.

NOMENCLATURE

A_{chip}	Cross Sectional Area of Chip
D_{cut}	Depth of Cut
D	Measured Depth of Wellbore
ECD	Equivalent Circulation Density
F_{cutter}	Cutter Force
$Grad_{water}$	Water Gradient
m	Slope of Mohr Envelope
MSE	Mechanical Specific Energy
MW	Mud Weight
P_H	Hydrostatic Pressure
P_P	Pore Pressure
PPG	Pounds per Gallon
PSP^3	Principal Stress Pore Pressure Prediction
R_{bit}	Radius of the Bit
r_c	Radius of Mohr Circle
ROP	Rate of Penetration
RPM	Revolutions per Minute
WOB	Weight on Bit
σ	Normal Stress
σ_1	Minimum Principal Stress

σ_3	Maximum Principal Stress
σ_C	Cutter Stress
σ_x	Normal Stress in x-direction
σ_y	Normal Stress in y-direction
τ_{xy}	Shear Stress

TABLE OF CONTENTS

LIST OF FIGURES

FIGURE Page

CHAPTER I

INTRODUCTION

Lost time events caused by unknown formation pore pressure, including blowouts, loss of circulation, and decrease in drilling rate, costs oil companies millions of dollars per annum. A more detrimental effect of unknown formation pore pressure is reservoir damage. This is caused by overpressure during drilling which results in damage of near wellbore permeability. The loss in permeability results in a significant decrease of production for each well or requires further investment to more effectively produce the formation. In an effort to reduce the cost of drilling an oil well and increase reservoir production, British Petroleum (BP) has teamed with Texas A&M Department of Mechanical Engineering to develop methods to predict pore pressure.

In industry today, companies are utilizing Mechanical Specific Energy (MSE) to determine the efficiency of a drill bit. More generally, they are determining the environment in which the bit is drilling by the processing of currently recorded drilling measurements.

An investigation was conducted to determine if similar drilling measurements could be processed to predict pore pressure. Through the investigation, a theoretical basis was developed that relates drilling measurements to the downhole stress state.

This thesis follow the style of the *SPE Journal.*

From the stress state, a prediction of pore pressure can be calculated. The new concept has been termed Principal Stress Pore Pressure Prediction (PSP^3). From the theoretical basis, a test procedure was created that converted industry drilling log data to the PSP^3. To verify the concept, the calculation process was then applied to three different wells and compared to actual pore pressure predictions.

In this report, the theoretical basis will be presented first in the Theory section. Then, the test procedure will be explained. Following this, the results of applying the test procedure will be presented and discussed. Finally, conclusions about the results and future recommendations for advancement of the project will be presented.

CHAPTER II

THEORY

Mohr's Theory

To represent the stress state of the bottom of the borehole, Mohr's Theory was applied. Mohr's Theory is a graphical representation of the stress state of an element under normal and shear stress. **Fig. 1** shows a two dimensional element in normal and shear stress.

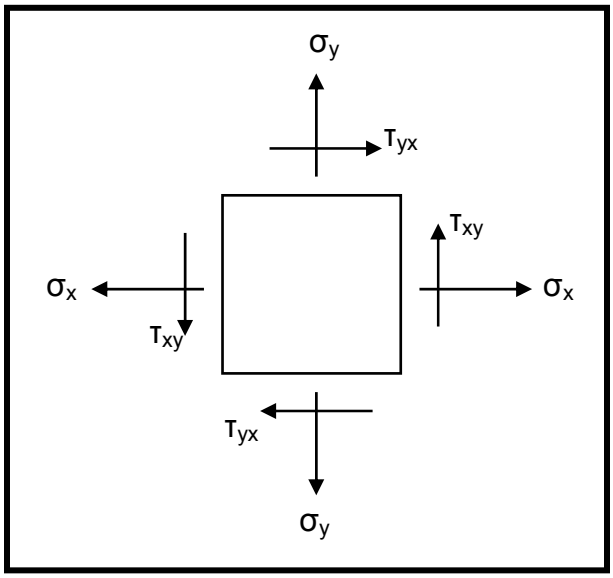

Fig. 1: Element in a State of Stress

In the figure, the normal stresses are σ_x and σ_y and the shear stresses are τ_{yx} and τ_{xy}. The graphical representation of the element in Fig. 1 is seen in **Fig. 2**,

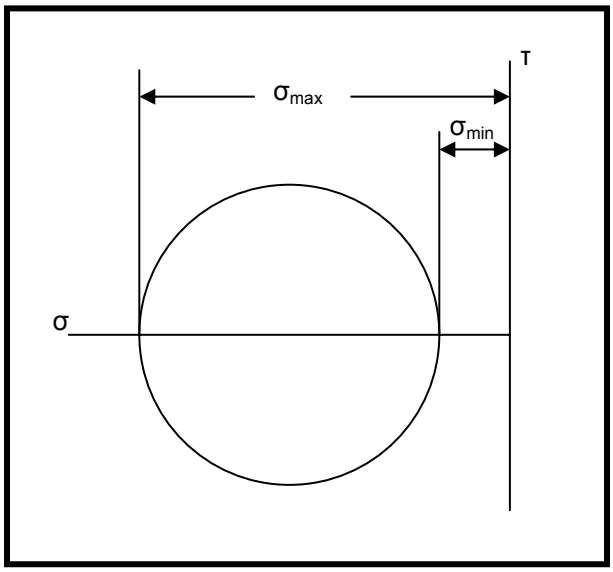

Fig. 2: Mohr's Circle of Stress Element

where the intersection of the principal stress axis (σ) and Mohr's Circle farthest from the origin is the maximum, principal stress (σ_{max}). At this state, shear stress is not being applied to the element and the largest normal stress is equal to the principal stress. The other intersection of the primary stress axis with Mohr's Circle is the minimum, principal stress. Also at this state, shear stress is not being applied to the element and the smallest normal stress is equal to the principal stress.

Mohr's Theory can also be applied to a three dimensional element, as seen in **Fig 3**. If only principal stresses are applied to the element, the Mohr's Circle representation can be created and is shown in **Fig. 4**.

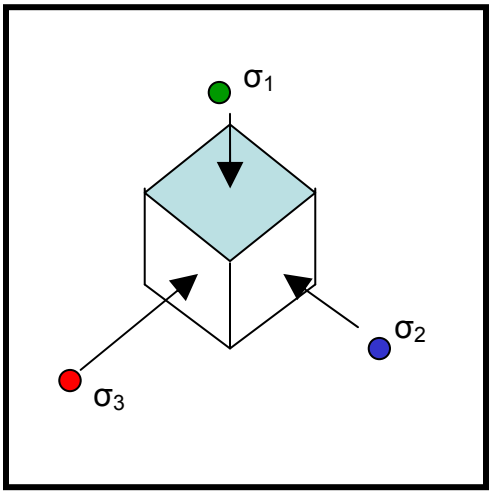

Fig. 3: Three Dimensional Stress Element

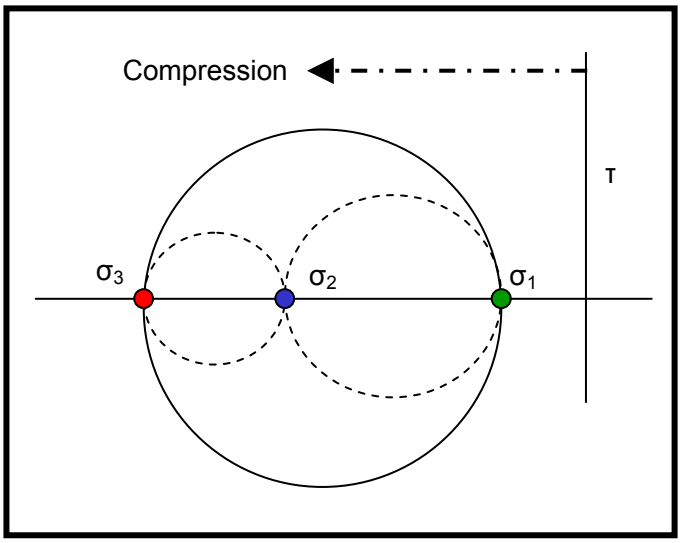

Fig. 4: Mohr's Circle Representation of a Three Dimensional Element

In the Mohr's Circle representation, all stresses are assumed to be in compression. The maximum stress is defined as σ_3, and the minimum stress is defined as σ_1. As can be seen in Fig. 4, to draw the outer Mohr circle only the maximum and

minimum, principal stresses need to be defined. The third stress, which lies on the range $\sigma_3 \leq \sigma_2 \leq \sigma_1$, does not need to be defined.

Mohr's Envelope

The strength of rock specimens is often found experimentally by inserting a cylindrical rock specimen in a press and loading the specimen until it fractures. The amount of load required to break the rock specimen is defined as its compressive strength. Stress can also be applied to the sides of the specimen during testing. This applied stress is defined as the confining stress as referenced by Obert and Duvall (1967). When the specimen is loaded on three different axes, the test is termed a "tri-axial test". **Fig. 5** shows a rock specimen and the stresses being applied to it.

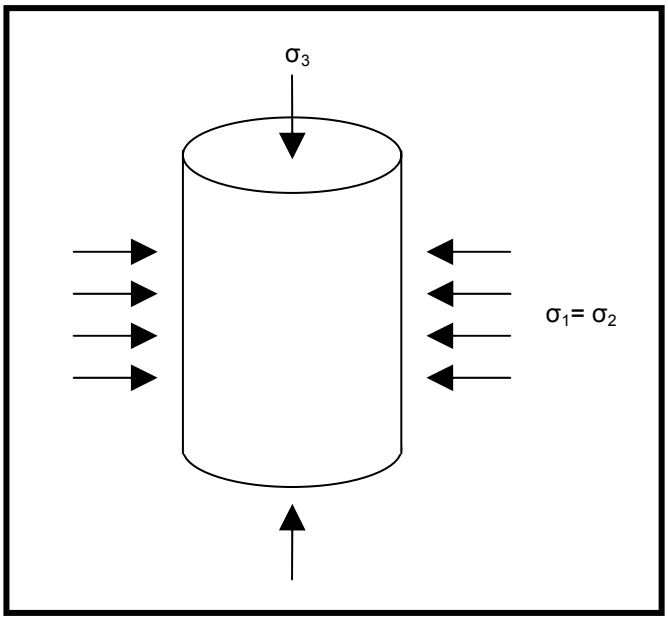

Fig. 5: Tri-axial Test

As the confining pressure (σ_1 and σ_2) is increased, the compressive stress (σ_3) needed to fracture the rock also increases. In the test, the maximum stress will always be σ_3 and the minimum stresses, σ_1 and σ_2, are equal. Since these are the only stresses applied, a Mohr's Circle representation can be made. If the tri-axial tests of increasing confining stress and the resulting σ_3 required to break the specimen are plotted as Mohr's Circles, **Fig. 6** can be developed.

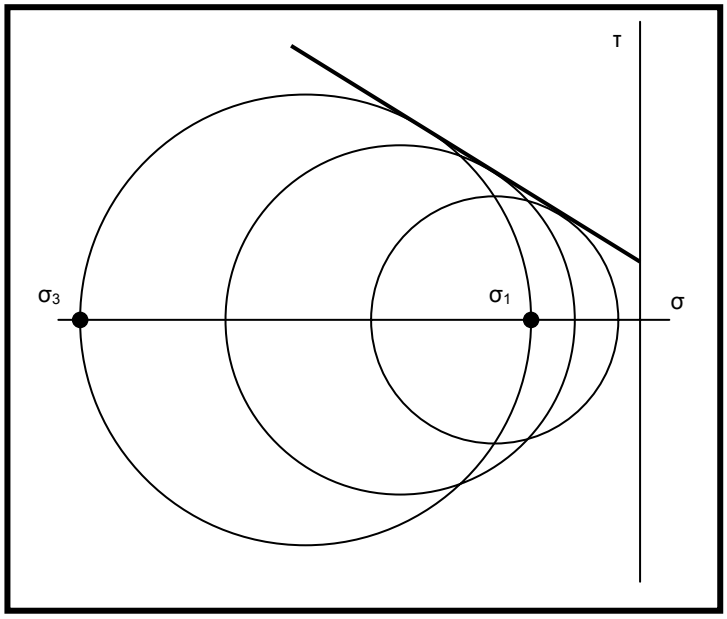

Fig. 6: Mohr's Envelope for a Series of Tri-axial Test Specimens

In Fig. 6, each circle is the graphical representation of the rock specimen at fracture when different stress states are applied. In the figure, the line that tangentially intersects the Mohr's Circles is defined as the Mohr's Envelope. The envelope encompasses all the Mohr's Circles. It is also known that, when a Mohr's Circle

intersects the envelope, the graphical representation will be of a specimen at failure as shown by Obert and Duvall (1967).

A property of the Mohr's Envelope is that it is unique for different rocks. For each rock type, the Mohr's Envelope will have a different slope and intercept.

Downhole Stress State

To determine the link between the MSE (a function of drilling measurements) and the pore pressure, the stress state at the borehole bottom must be defined. To determine this stress state, a two dimensional model of the rock chip under stress is shown from Gerbaud, Menand, and Sellami (2006) in **Fig. 7**.

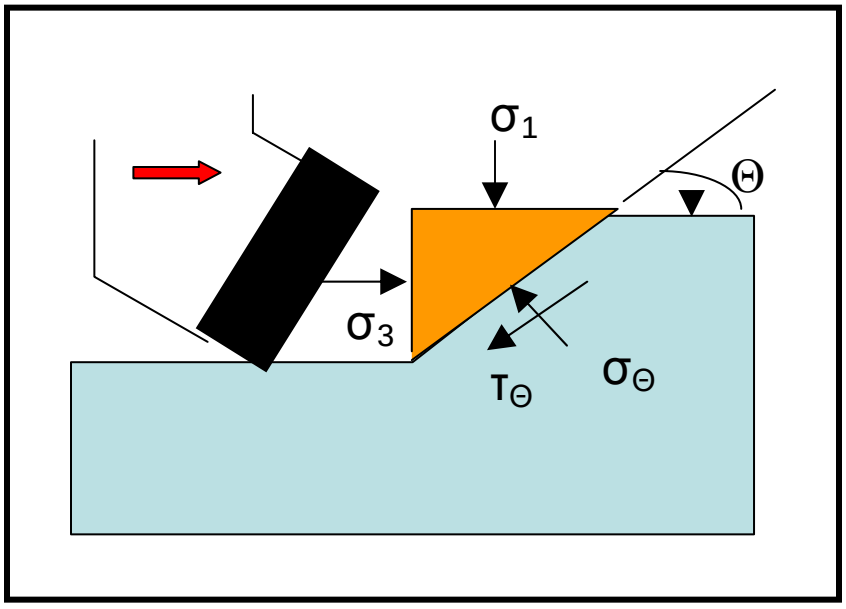

Fig. 7: PDC Bit and Rock Chip Schematic

The two dimensional model of the rock chip in the figure is similar to a tri-axial test. Following the terminology from the tri-axial test, the maximum, principal stress is defined by the horizontal stress applied to the chip (σ_3) because this applied stress breaks the rock chip away from the rock formation. Therefore from this definition, the minimum stress is then defined as the vertical stress (σ_1).

In the figure, the shear stress (τ_Θ) and the normal stress (σ_Θ) act along the slip plane defined by Θ. These two stresses correspond to the intersection of Mohr's Envelope and Mohr's Circle, shown in **Fig. 8**.

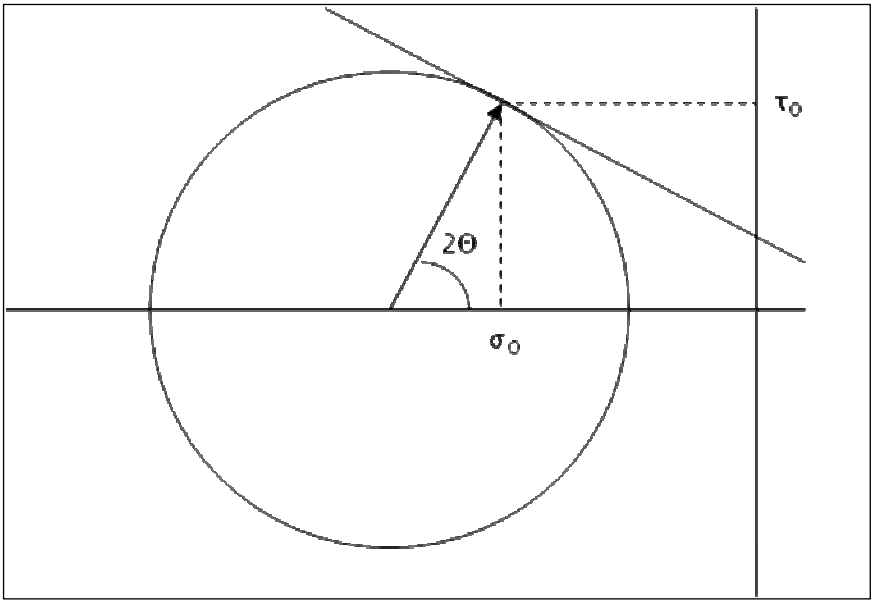

Fig. 8: Schematic of Slip Plane Stresses Defined by Mohr's Theory

Looking closer at the two dimensional model of the chip in Fig. 7, we can further define the different stresses being applied as:

- σ_3: Maximum Stress - Stress created by cutting force applied to cutting area and the pressure gradient
- σ_1: Minimum Stress - Stress created by the pressure gradient

The stresses that sum to equal the maximum and minimum stresses are represented in **Fig. 9**.

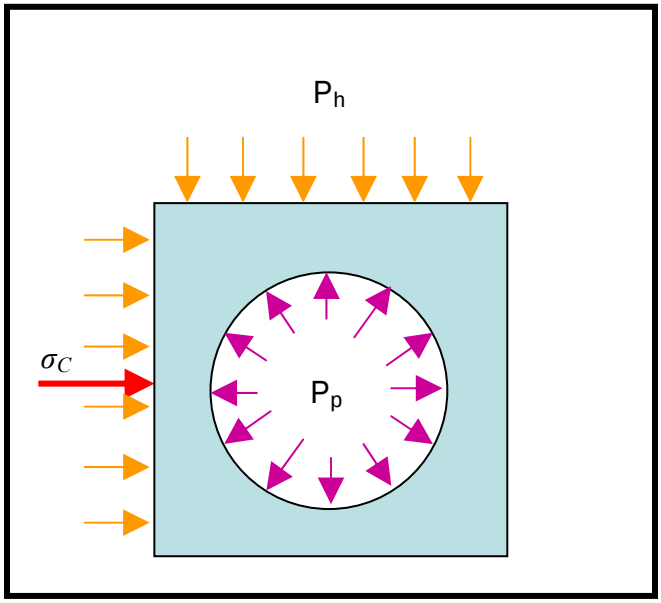

Fig. 9: Two Dimensional Stress Element of Chip with Pore

From the figure, the maximum stress (σ_3) in Fig. 7 is defined as the summation of the cutter stress (σ_C) being applied horizontally, the hydrostatic head (P_h) and the pore pressure (P_p). The stress applied vertically (σ_1) to the chip is defined by the summation of the hydrostatic pressure (P_h) and the pore pressure (P_p).

If a three dimensional stress element is considered, then the third stress (σ_2) is the confining stress on the element. This stress is a function of the load applied to the element by the overburden. Since this stress does not break the rock, it is assumed to be less than the maximum stress (σ_3). This stress is also assumed to be higher than the vertical stress (σ_1). Therefore, since the confining stress is defined as $\sigma_3 \geq \sigma_2 \geq \sigma_1$, then the confining stress is not required to draw the largest diameter Mohr's circle, as can be seen in Fig. 4.

Calculating Pore Pressure from the Stress State

From Fig. 9, the vertical stress σ_1 is defined by Eq. 1.

$$\sigma_1 = P_h + P_p \quad \text{..... (1)}$$

Therefore, if the hydrostatic pressure and the pressure differential (σ_1) are known, the pore pressure can be determined by Eq. 2.

$$P_p = \sigma_1 - P_h \quad \text{.....(2)}$$

Determining the Minimum, Principal Stress and Pore Pressure

To be able to determine the pore pressure from Eq. 2, the hydrostatic / pore pressure differential must be defined. From Mohr's Theory and the assumptions included in *Downhole Stress State*, there are several conclusions that can be deduced:

- σ_1 is defined as the minimum, principal stress on the largest diameter Mohr's Circle

- If Mohr's Circle intersects with Mohr's Envelope, then the stress element has reached the maximum stress state at fracture.
- When cutting, the horizontal force applied to the rock chip causes the chip to fracture from the formation.

From these conclusions, it is deduced that since the chip is at the maximum stress state during cutting, then the graphical representation of the chip is a Mohr's Circle that intersects the Mohr's Envelope. Therefore, using geometrical relationships, the minimum, principal stress can be found by knowing the cutter stress and Mohr's Envelope.

Finally, since the minimum, principal stress can be determined and the downhole pressure can be calculated, the pore pressure can be predicted by Eq. 2.

Determining Maximum, Principal Stress

The maximum, principal stress (σ_3) in the model is assumed to be the summation of the cutter stress, downhole pressure, and pore pressure as seen in Eq. 3.

$$\sigma_3 = \sigma_c + P_h + P_p \quad \text{.....(3)}$$

therefore, by substituting Eq. 1 into Eq. 3, Eq. 4 is derived.

$$\sigma_3 = \sigma_c + \sigma_1 \quad \text{.....(4)}$$

Eq. 4 is represented graphically in **Fig. 10**.

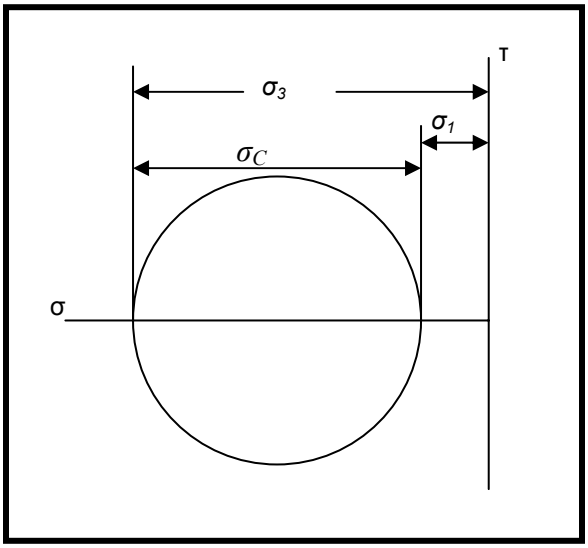

Fig. 10: Graphical Representation of Eq. 4

Eq. 3 contains three unknowns: cutter stress, downhole pressure, and pore pressure.

Determining Cutter Stress

The first unknown in Eq. 3 is the cutter stress. Stress has units of force applied to a cross-sectional area. Therefore, the cutter stress can be defined by Eq. 5.

$$\sigma_C = \frac{F_{cutter}}{A_{chip}} \quad \text{..... (5)}$$

The force of the cutter will be derived first, followed by the area of chip.

To derive the equation for force, the first assumption is that when a bit is cutting the formation, all teeth engaged are applying a stress larger than the compressive strength of the rock. Therefore, the rock breaks away from the formation. If the bit is cutting efficiently (absence of bit balling, missing teeth, etc), then all of the teeth will be

engaged simultaneously. If the bit is assumed to be fully engaged, then all the teeth of the bit can be combined to form an "effective tooth", as shown in **Fig. 11**.

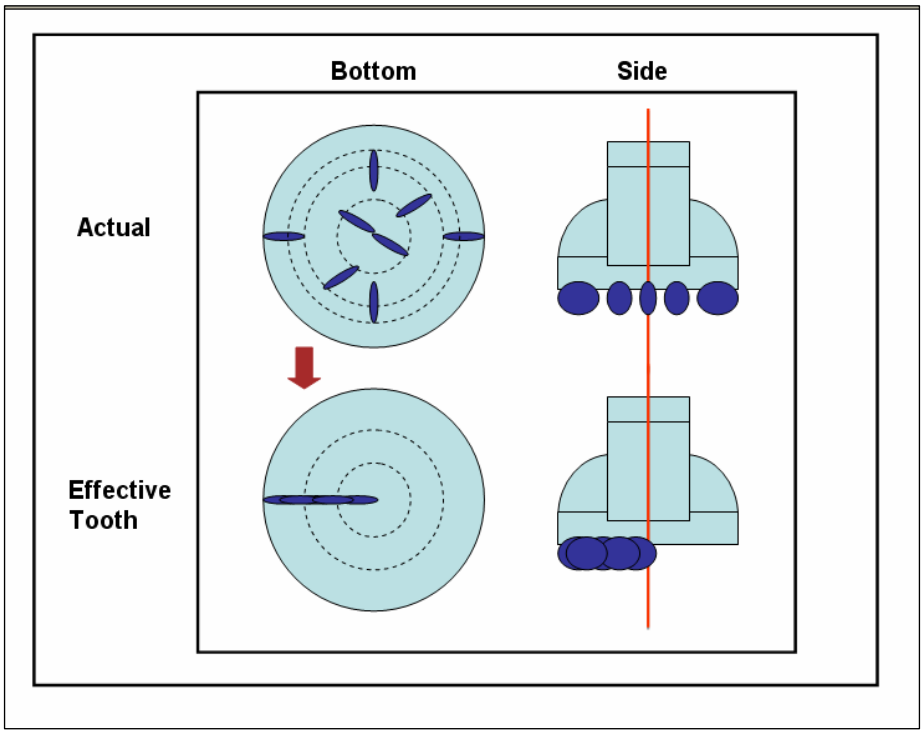

Fig. 11: Schematic of Combining Teeth to Form an Effective Tooth

The "effective tooth" will have the cross-sectional area of the distance from the center line of the drill-string to the outer diameter of the hole, by the depth of cut. This is seen in **Fig. 12**.

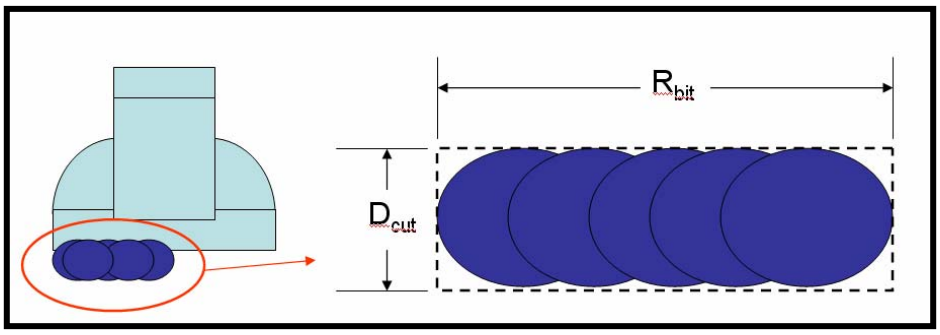

Fig. 12: Area of Effective Tooth

From these assumptions, the integral of torque over the tooth can be defined by Eq. 6 and rearranged to solve for the cutter stress. A schematic of the calculation is shown in **Fig. 13**.

$$T = \int_0^{R_{bit}} S_c \cdot D_{cut} \cdot r \cdot dr$$

$$T = \frac{S_c \cdot D_{cut} \cdot R_{bit}^{\,2}}{2}$$

$$S_c = \frac{2 \cdot T}{D_{cut} \cdot R_{bit}^{\,2}} \qquad \text{..... (6)}$$

where

σ_C = Cutter Stress Applied

T = torque from drilling log

R_{bit} = radius of the bit

D_{cut} = Depth of Cut

r = Moment arm from cylindrical center of bit.

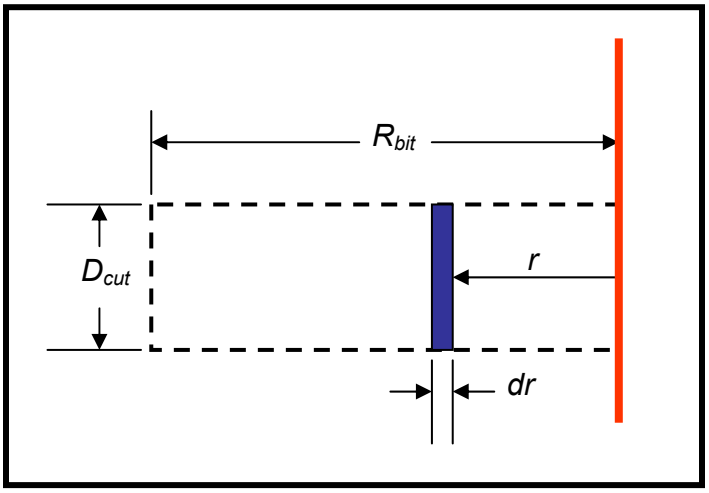

Fig. 13: Schematic of Torque Integral

From Eq. 6, the stress of the cutter can be determined. This stress is the difference between the maximum and minimum, principal stresses (Eq. 4). All variables of Eq. 6 are currently recorded during drilling except the depth of cut (D_{cut}). In the next section, the depth of cut will be derived.

Calculating Depth of Cut

The depth of cut must be determined to calculate the cross-sectional area to which the cutting force is applied. The penetration of the teeth from the drilling data is a function of volume of material removed and number of rotations. Therefore, the depth of cut is defined by Eq. 7.

$$D_{cut} = \frac{ROP}{RPM \cdot 2\pi} \quad \text{.....(7)}$$

where

ROP = Rate of Penetration

RPM = Revolutions per Minute.

To be able to determine the pore pressure, a final calculation must be made. From Eq. 2, to determine the pore pressure hydrostatic pressure must defined.

Calculating the Hydrostatic Pressure

Hydrostatic pressure at the bottom of the borehole is a function of the depth of the borehole, density of the mud, and gravitational constant. Drilling logs commonly plot mud density (mud weight) in pounds per gallon (PPG). However the downhole pressure while drilling also includes the added pressure created by the mud pumps. Therefore to calculate downhole pressure, the Equivalent Circulating Density (*ECD*) is a better approximation for mud weight. *ECD* adds a correction for increased pressure applied downhole by the mud pumps. Hydrostatic pressure is defined in Eq. 8.

$$P_h = ECD \cdot \frac{Grad_{water}}{Density_{water}} \cdot D \quad \text{.....(8)}$$

where

ECD = Equivalent Circulation Density (from drilling log)

$Grad_{water}$ = Fresh Water Gradient (Constant)

$Density_{water}$ = Density of Fresh Water (Constant)

D = Depth of borehole (from drilling log)

After calculating the cutter stress, depth of cut, and hydrostatic pressure, all parameters needed to calculate the pore pressure are known. Next, the graphical relationships needed to determine the pore pressure from drilling log parameters and Mohr's Theory will be derived.

Graphical Relationships

When the rock chip is at a failure state, Mohr's Circle will tangentially intersect with Mohr's Envelope. Since the diameter of Mohr's Circle is known (from σ_c), the circle can be translated along the principal stress axis until a solution is reached. A graphical representation of the desired solution is depicted in **Fig. 14**.

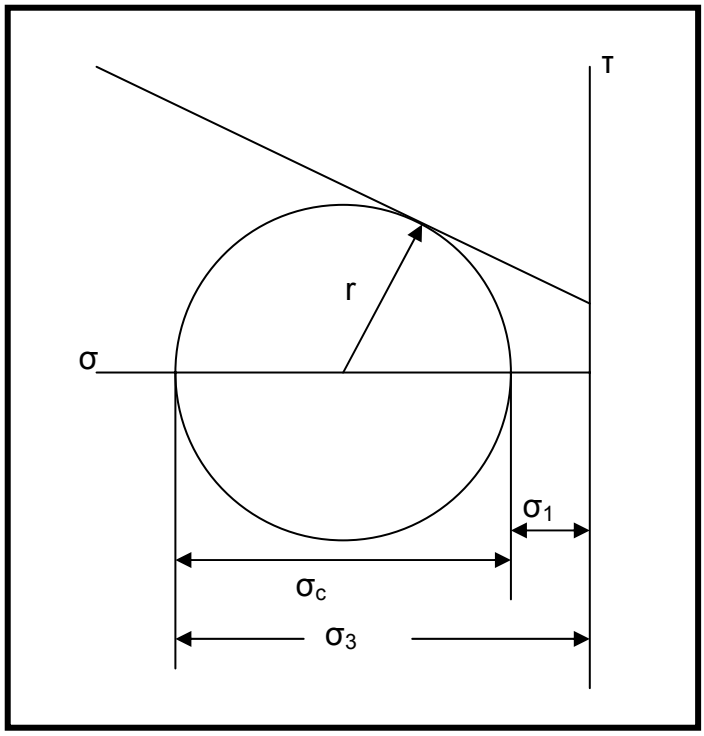

Fig. 14: Mohr's Circle Intersecting Tangentially with the Mohr's Envelope

In the figure, the graphical relationship between the circle radius, minimum and maximum principal stresses, and cutter stress are defined by Eq. 4 and Eq. 9.

$$r_c = \frac{\sigma_C}{2} \quad \text{.....(9)}$$

If segment lengths are defined in **Fig. 15** as,

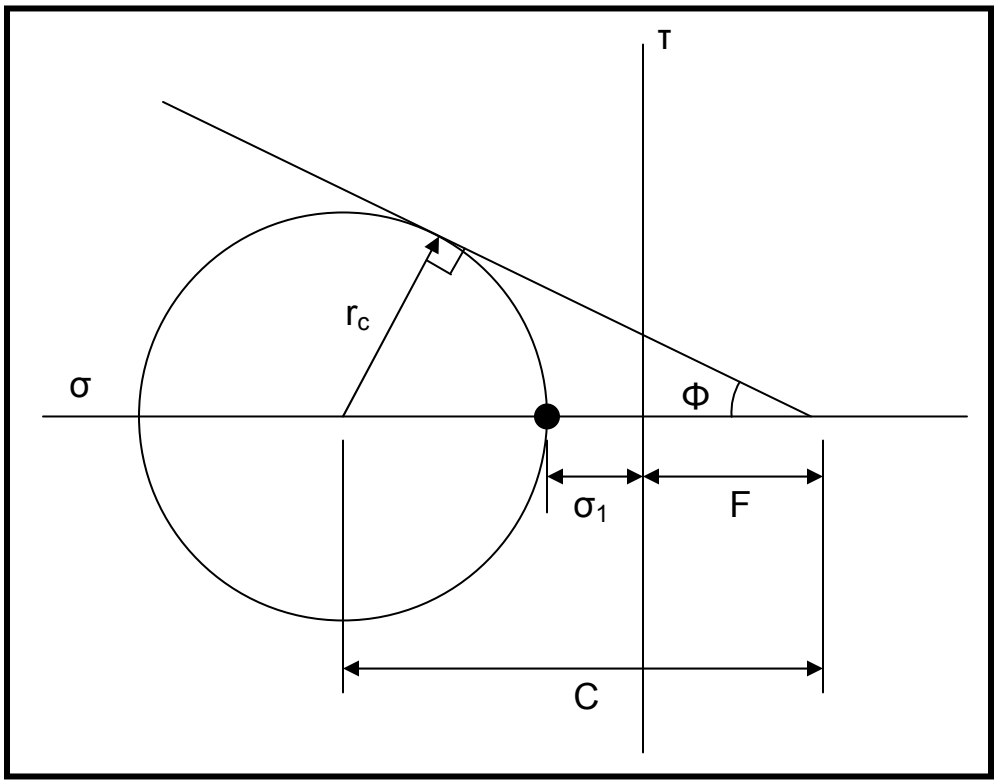

Fig. 15: Schematic Defining Graphical Relationships

then the relationship between the radius and the minimum principal stress can be defined by Eq. 10.

$$\sigma_1 = C - F - r_c \quad \text{.....(10)}$$

Using the equation of the Mohr's Envelope, *F* can be determined to be the distance between the intersection with the normal stress axis and the origin by Eq. 11.

$$\begin{aligned} &\tau = m \cdot \sigma + b \\ &\text{when } \tau = 0 \\ &F = \sigma = \frac{-b}{m} \end{aligned} \quad \text{.....(11)}$$

From the equation of Mohr's Envelope and the law of sines and cosines, σ_1 can be further defined by Eqs. 12 and 13.

$$\begin{aligned} &\sin \Phi = \frac{r_c}{C} \\ &\Phi = \tan^{-1}(-m) \\ &\sin\left(\tan^{-1}(-m)\right) = \frac{r_c}{C} \\ &C = \frac{r_c}{\sin\left(\tan^{-1}(-m)\right)} \end{aligned} \quad \text{.....(12)}$$

Substituting Eqs. 9, 11, and 12 into Eq. 10 yields Eq. 13.

$$\sigma_1 = \frac{\sigma_c}{2}\left(\frac{1}{\sin\left(\tan^{-1}(-m)\right)} - 1\right) + \frac{b}{m} \text{.....(13)}$$

With the minimum, principal stress defined, the pore pressure prediction can be determined by substituting Eq. 13 into Eq. 2 to form Eq. 14.

$$P_p = \frac{\sigma_c}{2}\left(\frac{1}{\sin\left(\tan^{-1}(-m)\right)} - 1\right) + \frac{b}{m} - P_h \text{.....(14)}$$

CHAPTER III

TEST PROCEDURE

With the theory and required equations defined, a sequential test procedure is needed to predict the pore pressure from the drilling log data. The following steps define a sequential test procedure to predict PP:

- The type of lithology being drilled is determined from the drilling and mud logs.
- A Mohr's Envelope is selected that corresponds with the lithology.
- The equation of Mohr's Envelope is found.
- From Eq. 14, the pore pressure is predicted.

The next section describes the results when the sequential process was applied to industry drilling data.

CHAPTER IV

RESULTS

Wells 1 and 2

To verify the concept, the test procedure was applied to drilling log data from industry. However due to incomplete understanding of the calculation process, the test procedure was altered during the primary test. In the altered procedure, the cutter stress was assumed to be the maximum stress. From geometrical relationships, the minimum, principal stress was then found. This calculation process was incorrect. However, error in the calculation process did not change the final conclusion of the concept. Further explanation will be included in the *Discussion of Results* section.

The first step in executing the procedure was to determine the type of rock that was drilled. In the first set of data given, the exact lithology that was drilled was not recorded on the drilling log or the mud log. Therefore, an exact Mohr's Envelope representation of the formation that was drilled could not be known. However to verify the concept, a Mohr's Envelope of Berea Sandstone was used to represent the lithology in a sandstone interval. Tri-axial data from Handin, Hager, Friedman, and Feather (1963) was used to create the Berea Sandstone Mohr's Envelope.

The sandstone depth interval selected for processing was determined by interpreting the gamma ray measurement on the drilling log. From the interpretation, a one hundred foot depth interval was selected. The input data in the interval had several

bad data points (NULL values taken by the instruments). These data points were filtered from the data set.

To verify the concept, a prediction of the pore pressure created by a post drill pore pressure analysis was plotted with the PSP^3.

When the test procedure was applied to the drilling data, **Fig. 16** from Well 1 was created.

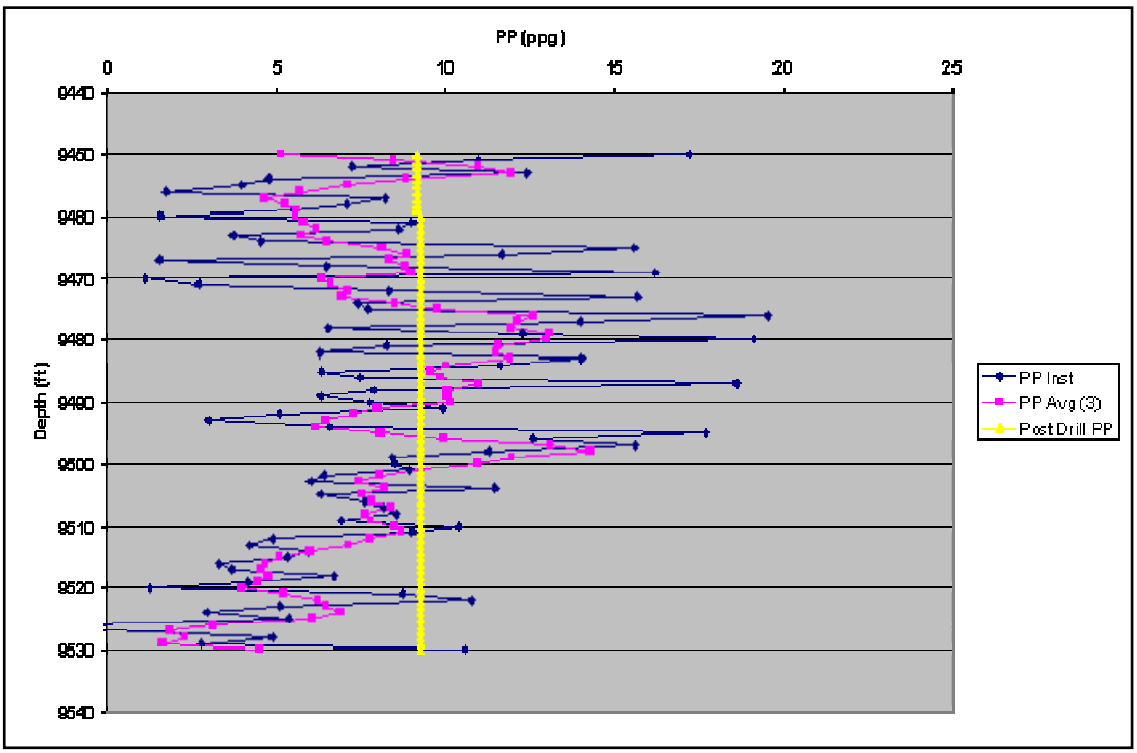

Fig. 16: PSP^3 for Sandstone Interval (Well 1)

In the figure, the blue data points are the PSP^3 at every foot interval, the pink data points are a moving average of the previous three PSP^3 data points, and the yellow is the prediction created from the post drill pore pressure analysis.

If the same Mohr's Envelope could be applied to the whole well, then implementation in industry would be executed with greater ease. Therefore, the Berea Sandstone Mohr's Envelope was used with the test procedure for the whole well to try to find a general Mohr's Envelope.

The calculation process was applied to data sets from 9,000 ft to 18,000 ft depth. From the resulting data, the calculations produced values with a variance from -100 to 100 PPG.

In an effort to find a more general Mohr's Envelope, the slope and intercept were modified. As these parameters were modified, the output of the prediction was monitored for reactions to the changes.

As the slope was increased, the data became more consolidated to within a couple PPG of mud density. A slope increase from 0.75 to 10 produced **Fig. 17**.

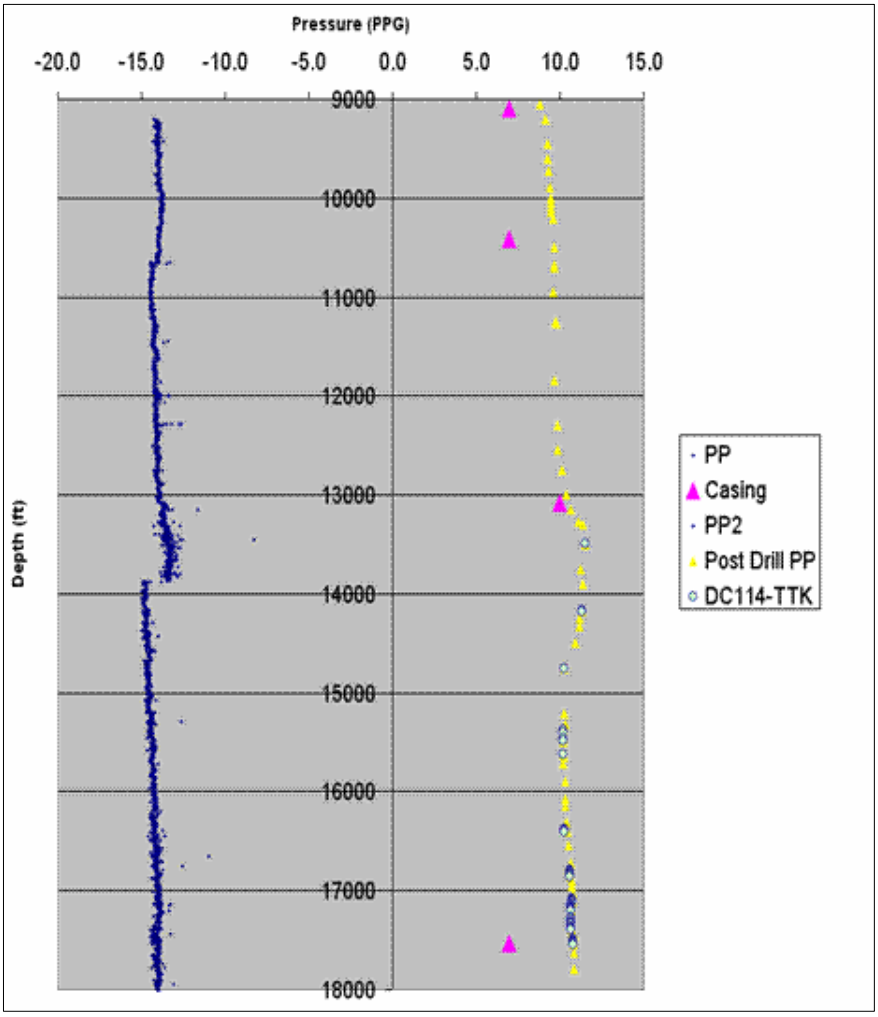

Fig. 17: PSP^3 with a Mohr's Envelope Slope of 10 (Well 1)

In the figure, the blue data points are the PSP^3, the yellow data points are the post drill pore pressure analysis, and the pink triangles are the casing shoe depths.

To better determine how the PSP^3 related to the actual pressure, the PSP^3 curve was shifted in the positive direction until it overlaid the actual measurements. With this shift, **Fig. 18** was produced.

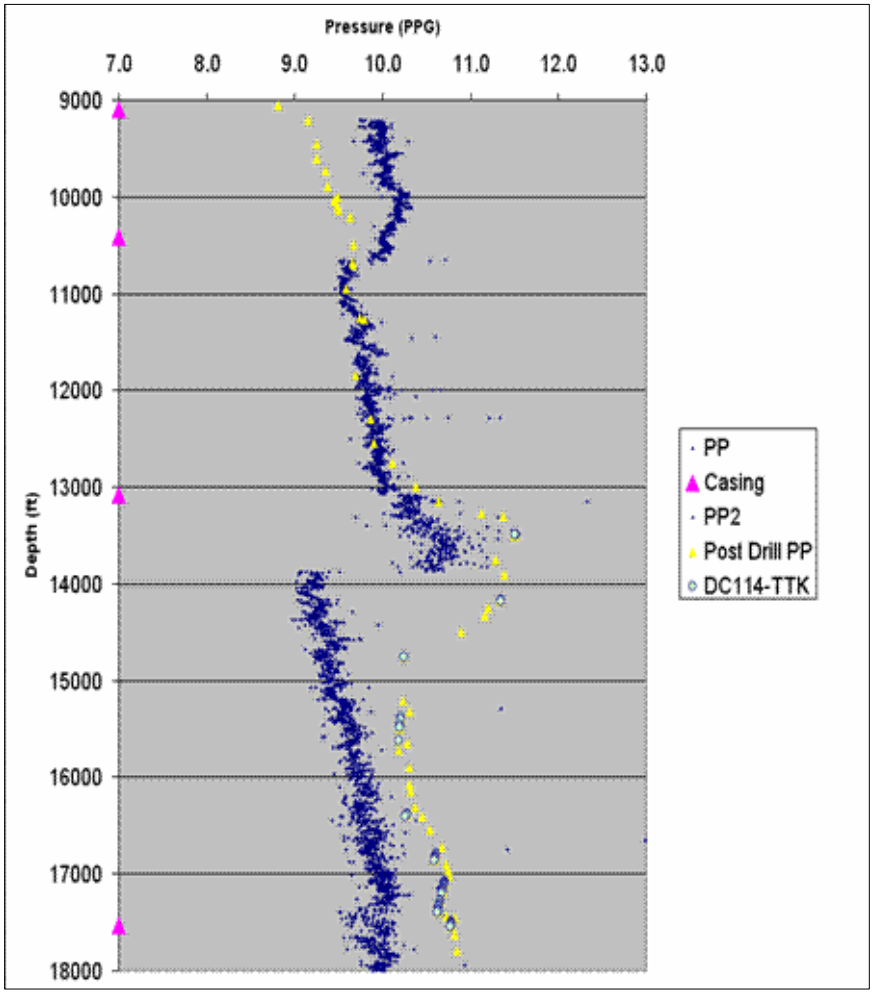

Fig. 18: PSP^3 with Mohr's Envelope Slope of 10 and +25 PPG Shift (Well 1)

As seen in the figure, the PSP^3 trended closely with the post drill prediction, however there are large jumps at the casing shoe depths.

A correlation between the required PSP^3 shift and the drill bit diameter was conducted. The correlation was plotted to produce **Fig. 19**.

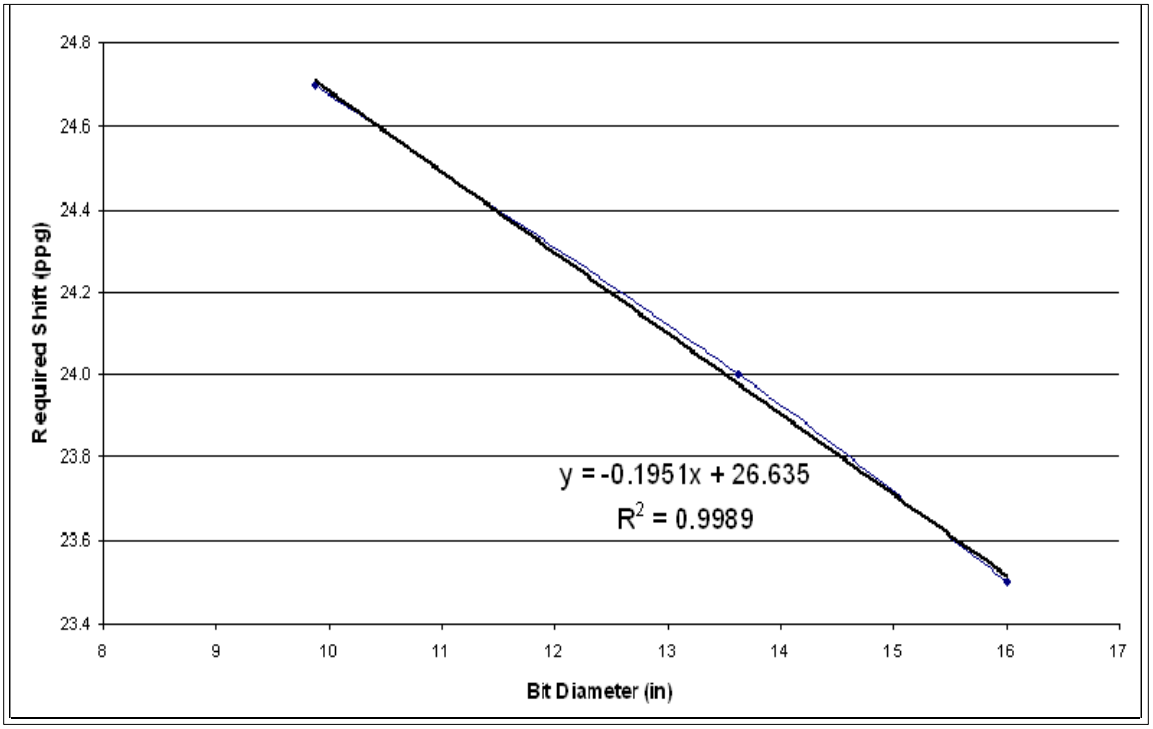

Fig. 19: Correlation between Required Shift of the PSP[3] as a Function of the Bit Diameter

The correlation produced a linear trend with a R^2 value of 0.9989. When the required shift was added to the PSP[3], **Fig. 20** was produced for Wells 1 and 2.

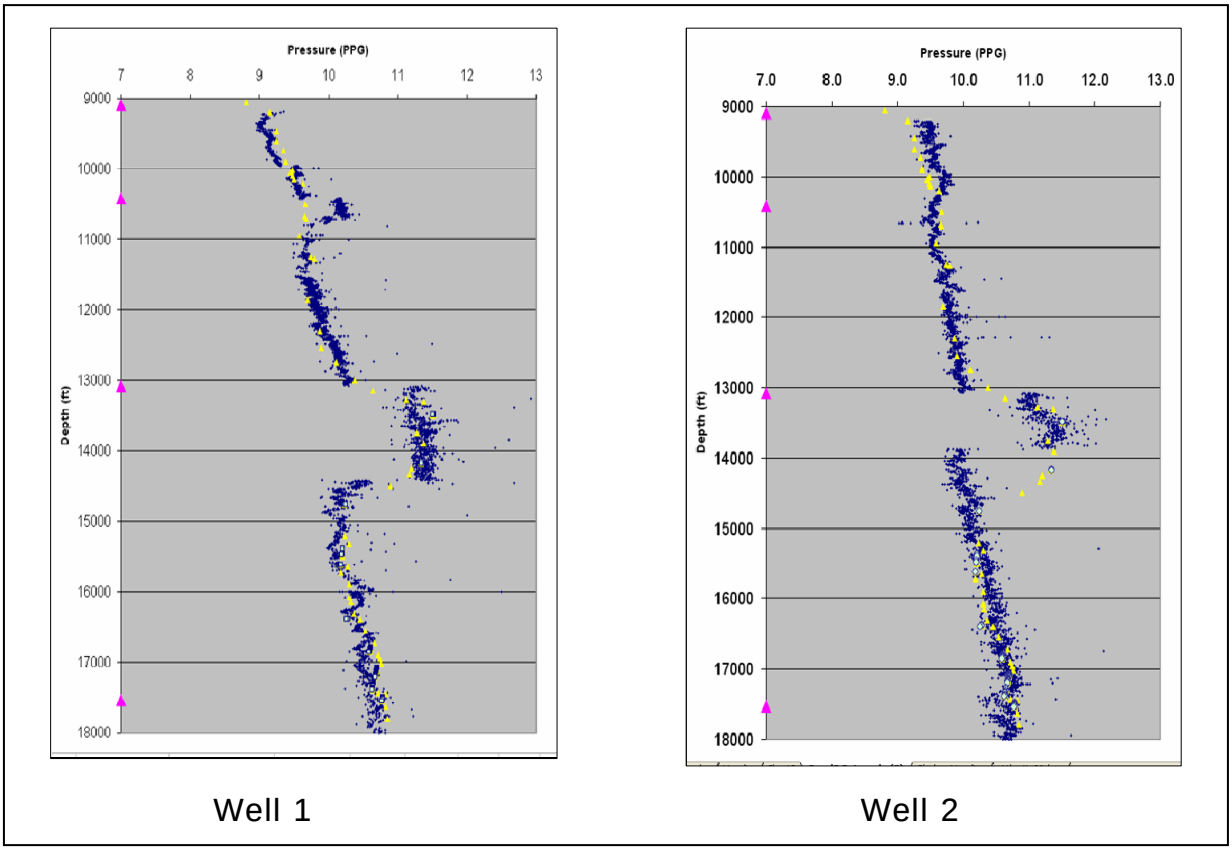

Fig. 20: PSP[3] for Two Wells in Same Play

For validation, the test procedure was then applied to another well in a different play.

Well 3

To validate the concept, the calculation process was applied to a third set of data from a different play. The same modified Mohr's Envelope (m=10) from Wells 1 and 2 was used. The result is seen in **Fig. 21**.

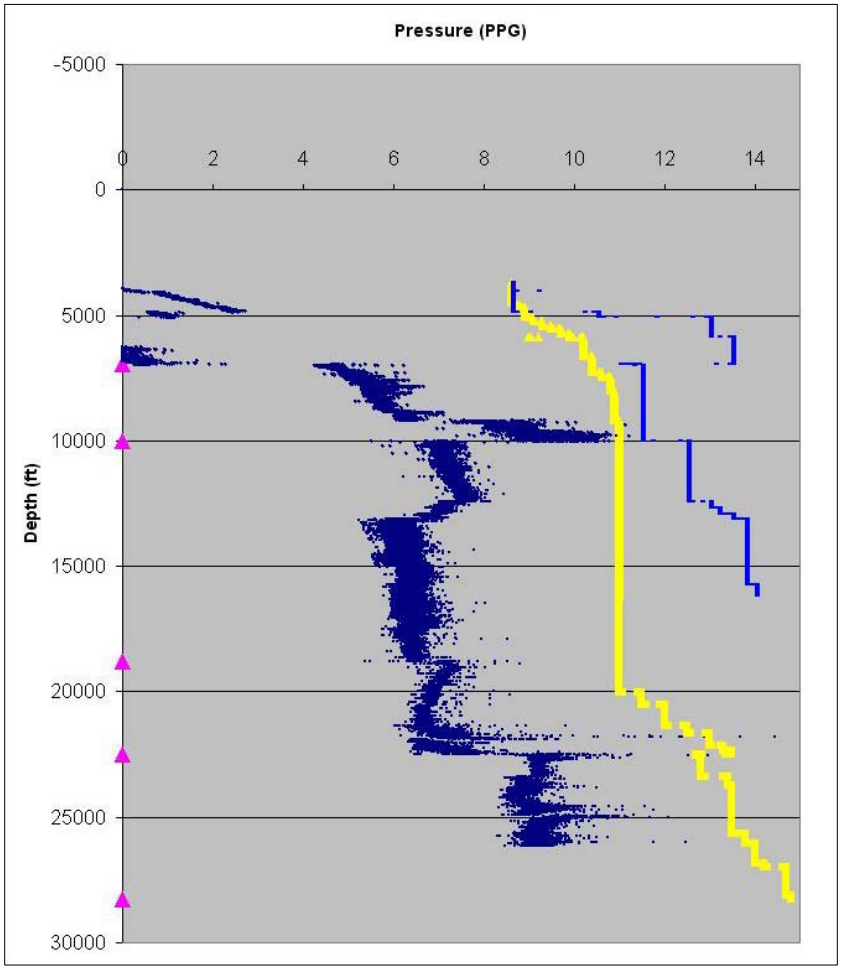

Fig. 21: PSP[3] and Mudlogger's P_P Estimation of Well 3

In the figure, the dark blue data is the PSP[3], the yellow data points are the mudlogger's prediction of P_P, the light blue data is the mud weight, and the pink triangles are the casing shoe depths. The P_P prediction for comparison is not as accurate as the post well analysis from Wells 1 and 2. However, the PSP[3] remains a couple of PPG below the prediction.

For the proceeding results, the cutter stress was assumed to be the maximum, principal stress in the calculation. This is an error in the calculation, but it does not

change the final conclusions about the concept. To verify this, the correct calculation process, outlined in *Theory and Test Procedure*, was applied to Well 1. The PSP^3 measurement can be seen in **Fig. 22**.

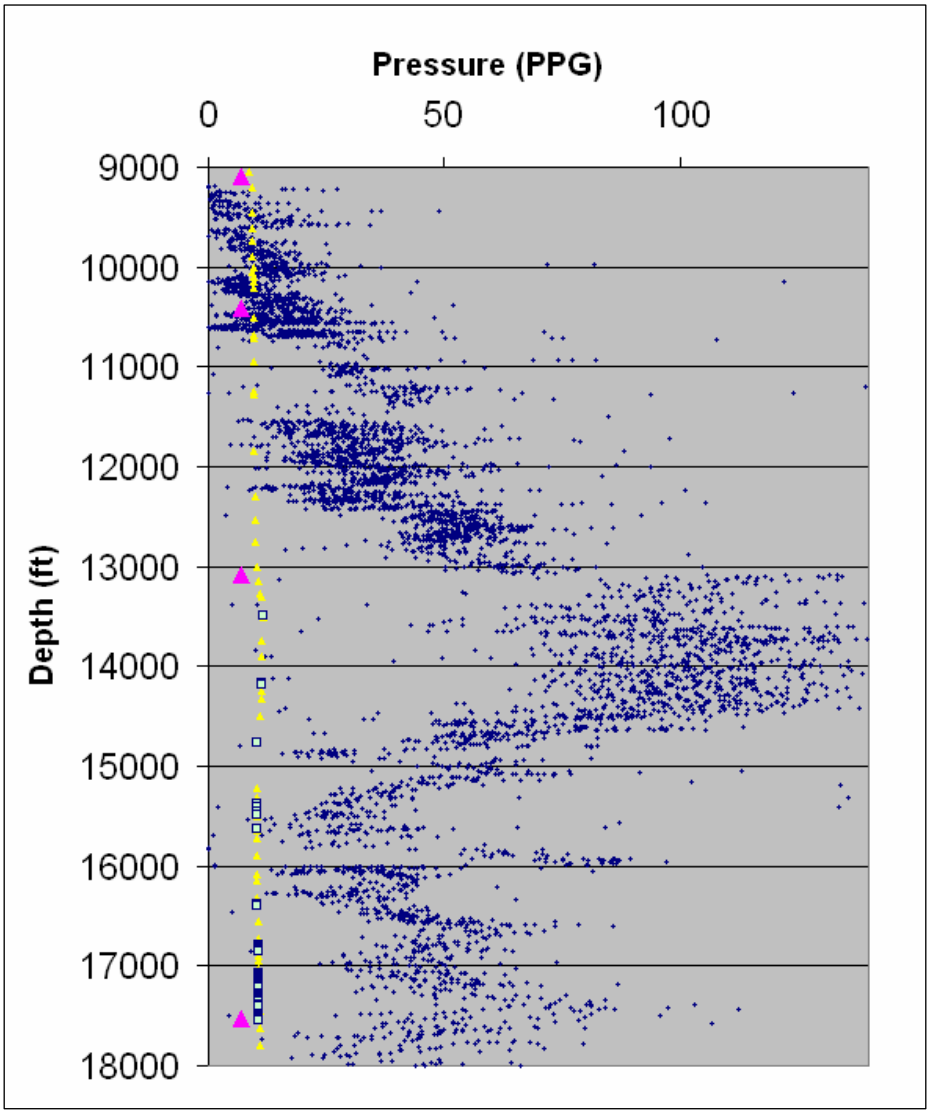

Fig. 22: PSP^3 for Well 1 Using Correct Calculation Method

In the figure, the blue data is the PSP[3], the yellow data points are the post drill pore pressure analysis, and the pink triangles are the casing shoe depths. For this calculation, the Mohr's Envelope for Berea Sandstone was used.

From the results produced by processing the drilling data, several important observations can be made. These observations are included in *Discussion of Results*.

CHAPTER V

DISCUSSION OF RESULTS

Raw data from three different wells was processed using the PSP^3 test procedure. The first PSP^3 was of a one hundred foot sandstone interval. The interval was determined by interpreting the gamma log. The PSP^3 is plotted with the post drill prediction in Fig. 16. From this plot, the PSP^3 has a range from 0 to 20 PPG mud weight (MW). To reduce the sensitivity of the prediction, a moving average of the previous three data points was also computed. This average is centered about the post drill prediction, yet has a 5 to 15 PPG MW variation. The PSP^3 method was then applied to the whole wellbore. When the test procedure was applied to the whole wellbore (9000 ft – 18,000 ft), the PSP^3 had a large variance similar to the sandstone interval.

The Mohr's Envelope of Berea Sandstone was then modified (slope and intercept) to determine if a general Mohr's Envelope for the whole wellbore could be found. With an increase in slope, the PSP^3 data points became more consolidated to within 1 PPG variation. This consolidated PSP^3 curve can be seen in Fig. 17. When the slope of the envelope was increased by an order of magnitude, it did not represent the failure envelope of the formations. The increase in slope actually reduced the minimum, principal stress and de-sensitized the PSP^3 to the fluctuations in torque.

As can be seen in **Fig. 23**,

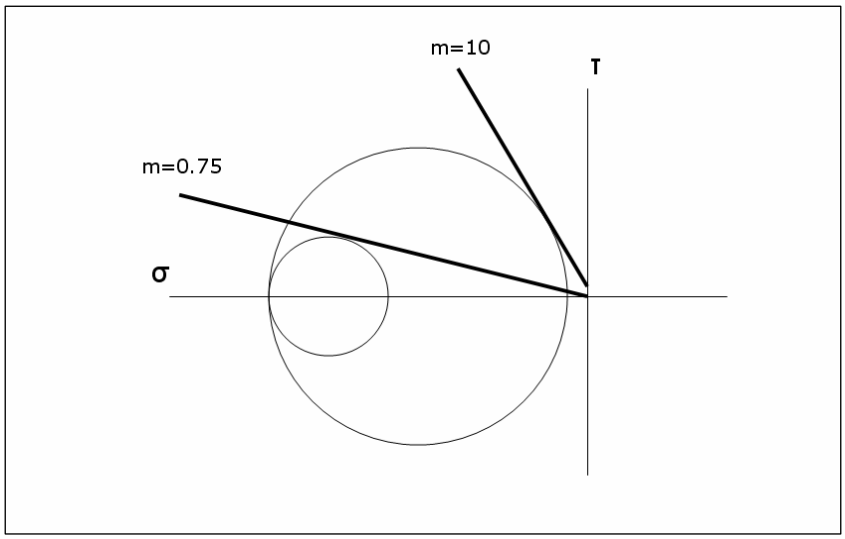

Fig. 23: Graphical Representation of Reducing the Minimum, Principal Stress by Increasing the Slope of the Mohr's Envelope

when the slope of the Mohr's Envelope is increased, the minimum, principal stress is reduced. It is important to note that as the slope goes to infinity, the minimum, principal stress goes to zero. The increase in slope of the Mohr's Circle also de-sensitizes the minimum, principal stress from the variations in torque. This can be seen in **Fig. 24**.

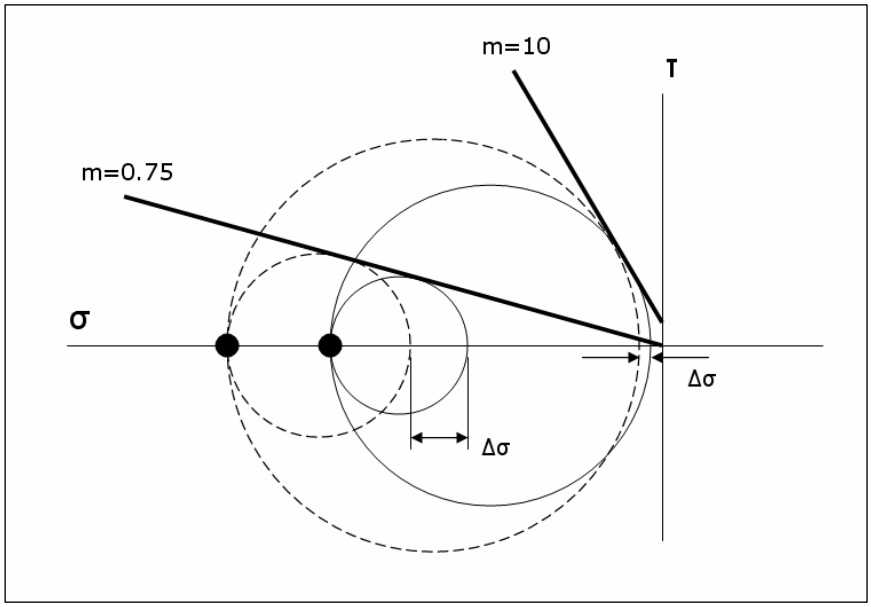

Fig. 24: Graphical Representation of De-sensitizing the Minimum, Principal Stress by Increasing the Slope of the Mohr's Envelope

In the figure, the Mohr's Circles are plotted with the same maximum stresses. The Mohr's Circles that intersect the envelope with m = 10, have a smaller variation in minimum stress ($\Delta\sigma$).

As the slope is increased, σ_1 goes to zero and Eq. 2 is approximated by Eq. 15.

$$P_p = -P_h \tag{15}$$

Therefore, the PSP^3 becomes only a function of mudweight. When the mudweight is plotted with the absolute value of the PSP^3 in **Fig. 25**, this result can be seen.

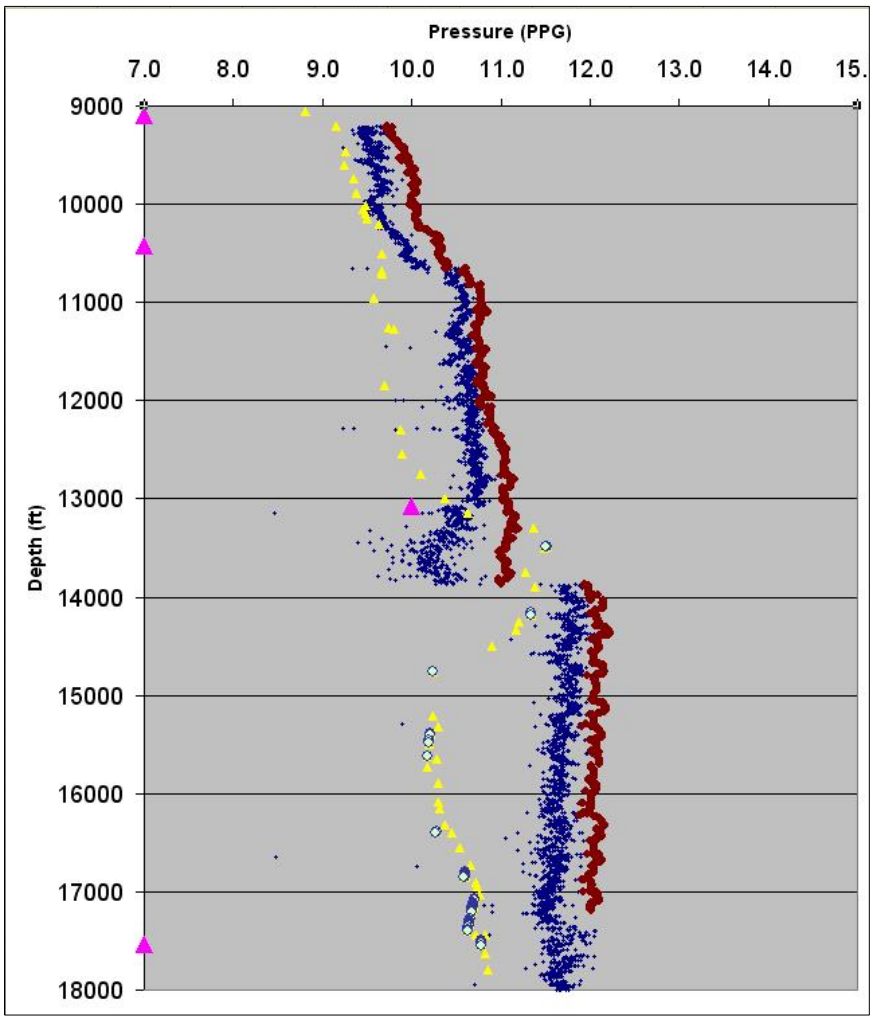

Fig. 25: Mud Weight Plotted with the Absolute Value of the PSP[3]

In the figure the blue is the PSP[3], the yellow is the post well pressure prediction, and the brown is the mudweight. It is important to notice that there are anomalies from 13,000 to 14,000 ft, where the PSP[3] varies from the mudweight as the pore pressure increases.

Due to the effect on the minimum, principal stress of increasing the Mohr's

Envelope slope, the concept is not proven valid by the results of applying the test procedure to the drilling data.

In Fig. 22, the results from applying the correct calculation method to the industry data are presented. The first observation is that the PSP^3 data points have a large amount of scatter. This scatter of data points is driven by the fluctuation of the drill string torque. Torque fluctuation is common during drilling due to the highly transient downhole environment. This environment includes many types of vibration including stick-slip, bit whirl, and unbalanced bits (missing teeth).

The second observation is that a correlation between the PSP^3 and post drill P_P could not be realized. The PSP^3 varies from 0 to 150 PPG while the post drill prediction remains within ±5 PPG of 10 PPG.

CHAPTER VI

SUMMARY

In summary, to develop and verify a possible solution, a theoretical basis was defined, a test procedure was created, and then the procedure was applied to industry data.

When the procedure was first applied to a sandstone depth interval, the PSP^3 had a range of approximately 0 to 20 PPG pressure, where the post drill prediction had a range between 8 and 9 PPG pressure.

While trying to find a more general Mohr's Envelope, it was found that when the slope was increased, the representation became invalid. Therefore, the primary results were invalid. When the correct test procedure was applied to the test data, the PSP^3 had a range from 0 to 150 PPG pressure. This large variation masked the actual pore pressure prediction.

The PSP^3 method has many benefits that make determining the validity of the concept attractive. First, the concept uses only equipment and measurements that are currently used in drilling. A new tool design is not required to implement the concept. Second, the concept's calculations can be completed quickly. This allows for the pore pressure prediction to be assessed continuously while drilling. Third, the concept can be quickly implemented in the drilling procedures. If the concept is validated, the PSP^3 could be plotted alongside torque, WOB, and other drilling measurements for the driller to view.

CHAPTER VII

CONCLUSIONS

Two conclusions can be made about the research. First, Mohr's Theory indicates that the PSP^3 model is valid. Second, the model cannot be disproved from the results because there was too much variation in the torque measurements.

CHAPTER VIII

RECOMMENDATIONS

To prove the concept, there are two issues that need to be resolved. The first issue is the large variation of the torque data. Due to this variation, the actual measurement of pore pressure is masked. The second issue is the number of effective blades, experienced by the formation downhole, needs to be determined. If it is found that the number of effective blades must be increased, the PSP^3 would converge to a closer value of pore pressure.

To accomplish this, the PSP^3 test procedure should be applied to controlled, experimental data. In a controlled environment, all required parameters could be measured without significant variation caused by unknown parameters. In the controlled experiment, the controlled parameters should include:

- Rock type and corresponding tri-axial test data
- Bit type and characteristic form (number of teeth, number of blades, diameter)
- Pore pressure applied to rock
- Wellbore pressure
- Torque
- Rate of Penetration (ROP)
- Revolutions per Minute (RPM)

The experimental data could be generated by either working with third party vendors or conducting a local experiment. Collaboration with a third party vendor might be a better decision because they conduct multiple tests for every bit that is produced. Therefore, the data may be currently available.

To determination the validity of the PSP^3 concept, the results must meet either of two criteria:

- The concept correctly predicts the pore pressure.
- A correlation between the pore pressure prediction and the actual pressure is found when a bit factor is applied to the calculation.

The bit factor could be function of effective number of blades, diameter of bit, angle of teeth, or other physical characteristics of the bit. Accuracy of the prediction should be within 1 PPG of the actual pore pressure. With this accuracy, PSP^3 could be implemented in industry.

REFERENCES

Gerbaud, L., Menand, S., and Sellami, H. 2006. *PDC Bits: All Comes From the Cutter/Rock Interaction*. IADC/SPE Drilling Conference, 21-23 Feb, Miami, Florida, USA. SPE #98988-MS.

Handin, J., Hager, R., Friedman, M., and Feather, J. 1963. *Experimental Deformation of Sedimentary Rocks Under Confining Pressure: Pore Pressure Tests.* Bulletin of the American Association of Petroleum Geologists. Volume 47 Number 5.

Obert, L. and Duvall, W. 1967. *Rock Mechanics and the Design of Structure in Rock,* New York City: John Wiley and Sons, Inc.

VITA

Name:	Kyle Wade Richardson
Address:	PO Box 1111, Ozona, TX 76943
Email Address:	kyle.w.richardson@gmail.com
Education:	B.S., Mechanical Engineering, Texas A&M University, 2006 M.S. Mechanical Engineering, Texas A&M University, 2008